LLNL-JRNL-402077

Solution-based characterization of surface-enhanced Raman response of single scattering centers

T. A. Laurence, C. Talley, A. Schwartzberg, G. Braun, M. Moskovits, N. Reich, T. Huser

March 8, 2008

Journal of the American Chemical Society

Disclaimer

Solution-based characterization of surface-enhanced Raman response of single scattering centers

Ted A. Laurence[A], Chad Talley[A], Adam Schwartzberg[A], Gary Braun[B], Martin Moskovits[B], Norbert Reich[B], Thomas Huser[C]*

[A]Chemistry, Materials, Earth and Life Sciences Directorate,

Lawrence Livermore National Laboratory, Livermore, CA 94550

[B]Department of Chemistry and Biochemistry, University of California, Santa Barbara, CA 93106

[C]NSF Center for Biophotonics Science and Technology, University of California, Davis, Sacramento, CA 95817.

*Corresponding author. E-mail: laurence2@llnl.gov.

RECEIVED DATE (to be automatically inserted after your manuscript is accepted if required according to the journal that you are submitting your paper to)

Abstract. We demonstrate the rapid optical characterization of large numbers of individual metal nanoparticles freely diffusing in colloidal solution by confocal laser spectroscopy. We find that hollow gold nanospheres and solid silver nanoparticles linked with a bifunctional ligand, both designed nanostructures, exhibit significantly higher monodispersity in their Rayleigh and Raman scattering response than randomly aggregated gold and silver nanoparticles. We show that measurements of rotational diffusion timescales allow sizing of particles significantly more reliably than can be obtained using translational diffusion timescales.

1 Introduction

Surface-enhanced Raman spectroscopy (SERS) has gained significant interest in recent years after potential enhancement factors over conventional Raman spectroscopy as high as 15 orders of magnitude have been reported [1, 2], enabling Raman experiments at the single molecule level and reinvigorating interest in SERS as an ultrasensitive biosensing platform. These significant enhancements have been attributed to a combination of effects, most significantly, the formation of nanoparticle dimer-like structures that enclose the molecules of interest in the gap between the nanoparticles [3-7]. The characterization of the optical properties of such SERS-active nanoparticles is a general requirement for optimizing their design through nanoengineering, and connecting specific designs to the general theory for nanoparticle-based SERS enhancement. Currently, this characterization is rather tedious and can only be performed for a few particles at a time. Multi-modal approaches are needed, where particles adhered to a surface are first probed for their optical response, and then correlated with transmission electron microscopy (TEM), scanning electron microscopy (SEM) or atomic force microscopy (AFM) to monitor size; see, for example [7, 8]. Here, we present an approach that allows us to characterize a large number of different parameters of individual nanoparticles simultaneously, under aqueous conditions;

we monitor particle size, polarization response, Raman activity, Rayleigh activity, and continuum background contributions on a per-particle basis.

Very strong enhancement of Raman scattering in SERS is typically correlated with the formation of aggregates or clusters. These enhancements result from the intense electric fields located within the junctions of the nanoparticle aggregates. Unfortunately, the ambiguity and heterogeneity in nanoparticle cluster formation leads to heterogeneity in their Raman enhancements. This heterogeneity can significantly reduce our ability to use SERS in a well-controlled manner for practical applications. Recently, metal nanoshells [8, 9] have been introduced that e.g. reduce the variability in the pH response of nanoparticle probes because they have been shown to provide significant Raman enhancement even at the level of individual particles. Additionally, nanoparticle clusters formed using the bifunctional Raman tag linker aminobenzenethiol (ABT), coated with a layer of PVPA, have been used to obtain very large Raman enhancements in a reproducible manner (G. Braun et al., personal communication).

Our group is developing functionalized SERS nanoparticles for measurements of the intracellular concentration of metabolites and metabolic indicators. Such nanoparticles are promising as probes because they are very photostable, active in the near-infrared region of the optical spectrum, and can relatively easily be probed and distinguished from the autofluorescence background from most cells. An elucidation of the properties that affect Raman enhancement and the overall optical response of nanoparticles and nanoparticle clusters may prove very useful in the development of better SERS-active substrates and probes.

For the rapid characterization of nanoparticle probes and their response to changes in their environment, a high-throughput method is needed. In order to test the optical response of nanoparticles within different parameters that may improve the homogeneity, many samples will need to be tested under similar environmental conditions. The standard practice of placing particles on a surface, and performing Raman spectroscopy particle by particle yields a large amount of information on individual particles. However, only a small number of particles can feasibly be probed in this manner. In particular, the temporal resolution for such characterizations is generally very limited, down to 30-100 ms at best.

An alternative approach to characterizing the spectroscopic properties of nanoparticle systems is to use particles that are freely diffusing in solution and apply correlation-spectroscopy-based techniques. Correlation techniques have been used for several years in fluorescence studies to characterize mobility, rotational diffusion, molecular interactions, and photophysical fluctuations. In single-molecule fluorescence studies (SMFS), immobilized molecules provide long-term trajectories on the order of several tens of seconds [10]. Solution-based studies contain less information per molecule, but are able to probe thousands of molecules within a short time, easily characterizing any subpopulations[11]. In an analogous fashion to SMFS, here we use solution-based methods to characterize nanoparticles diffusing in solution. Our experiments are similar in nature to those conducted by Eggeling et al.[12]with the omission of the lifetime spectroscopy and the addition of multiple channels monitoring narrow spectral ranges. Previous solution-based characterization of nanoparticles has focused on correlation spectroscopy over relatively wide spectral ranges. Here, we quantify the relative contributions of Rayleigh, Raman, and continuum background scattering using ratiometric variables and correlation spectroscopy. These techniques are shown to be effective tools in characterizing distributions of scattering particles. By comparing solid spherical gold nanoparticles of a uniform size, silver nanoparticles of varying size and shape, uniform hollow gold nanoshells, and clusters formed with bifunctional linkers, we show that the behavior of the scattering particles depends strongly on shape and structure. The changes in behavior are likely explained by variations in the spectral plasmon resonance response from particle to particle or particle cluster to particle cluster.

2 Materials and Methods

2.1 Samples

Four substrates are used and compared quantitatively for our scattering measurements. First, silver nanoparticles with a wide variety of sizes and shapes (typically 30-60 nm) are produced using the commonly used citrate reduction procedure from Lee and Meisel [13].

Second, the gold particles were made via the seed mediated growth method of Jana et al. [14]. First, 12 nm seed particles were grown via the Turkevich method. Briefly, 250 ul of a 0.1 M HAuCl4 aqueous solution was added to 100 ml of milli-Q water. This solution was brought to a boil under magnetic stirring and 3 ml of an aqueous 1% sodium citrate solution were added. Boiling was continued for 10 minutes after color change from yellow to dark red. The solution was allowed to cool and was reconstituted back up to 100 ml with water. Next, these particles were used for the seeded growth process. 2.25 ml of the as prepared gold seed particle solution and 244 ul of 0.1 M HAuCl4 were added to 148 ml milli-Q water. Under rapid stirring 100 ml of a 0.4 mM ascorbic acid solution was added slowly (~10 ml/min). The resulting sol contained approximately 50 nm gold particles with good homogeneity. These produce stronger signals than commercial preparations. We suspect this is due to a greater propensity for clustering or aggregation in our preparation, which has lead in parts to the current study.

Third, hollow gold particles were produced by the same method as published previously[8]. First, cobalt particles were formed as the deposition template. Briefly, 100 ml of water was placed in a 500 ml three-neck flask with 500 ul of a 0.1 M solution of sodium citrate and deoxygenated. To this, 300 ul of a freshly made 1 M sodium borohydride solution was added. With rapid magnetic stirring, 100 ul of a 0.4 M cobalt chloride solution was added rapidly. This solution was allowed to react for 20 minutes under constant argon flow until hydrogen formation was no longer observed, indicating complete hydrolysis of the reductant. To grow the gold shell, the borohydride free cobalt particles were used as synthesized. The argon flow was increased and under rapid stirring a 0.1 M HAuCl4 solution was added 50 ul per addition to a total volume of 500 ul. After each addition the solution was allowed to mix for several seconds to ensure good homogeniety upon addition. Upon completion the argon flow was ceased and the vessel was opened to ambient conditions under rapid stirring to oxidize any remaining cobalt metal left in solution. The peak of the plasmon resonance was near 600 nm, and the size of the nanoparticles was shown by TEM to be near 45 nm.

Fourth, the ~50 nm diameter silver nanoparticles of Lee and Meisel [13] were formed into clusters using a linker molecules. First, the nanoparticles were concentrated by centrifugation to twice the concentration in 10 mM sodium phosphate buffer pH 7.8. ABT in methanol (160 uM) was added to induce aggregation and caused a color change from yellow to green (requiring ~3 uM ABT) followed by addition of 20 uL polyvinylpyrrolidone in water (40 kDa, 1 mg/mL). Five minutes later two rounds of low speed centrifuging and redispersion in water was performed, each time discarding the yellow supernatant and any solids. The size distribution (by TEM) was centered around approximately 100 nm.

The measurements are performed on the samples as prepared, without dilution. No specific Raman signal is found for these pure nanoparticle samples. In order to achieve a specific Raman signal, we add 1-50 µl of 1 mM 4-mercaptobenzoic acid to 1 mL of sample to functionalize the nanoparticle surfaces. These were allowed to incubate at room temperature for 1-2 hours. Due to higher concentrations of the nanoshells, the concentration was increased to 50-500 µM to coat the surfaces.

2.2 Ratiometric spectroscopy of single nanoclusters

Individual light-scattering nanoparticles or small clusters of nanoparticles are allowed to diffuse freely in solution through the confocal detection volume defined by the focused laser and the pinhole in the experimental setup described in Figure 1. As shown in Figure 1a, excitation light from a 633 nm HeNe laser is reflected by a dichroic mirror (DM1, dual band dichroic reflecting 488 nm and 633 nm, Omega Optical, Brattelboro, Vermont). The laser excitation is focused into solution by a high numerical aperture microscope objective (60X 1.4 NA oil immersion Plan Apochromat, Nikon, Tokyo,

Japan), and bursts of photons scattered by nanoparticle clusters diffusing through the laser spot are collected by the same objective.

After passing through DM1, the tube lens (L1) focuses the scattered light onto a pinhole (PH) to exclude out-of-focus light. The scattered light is then collimated using an achromatic lens (L2). Two successive dichroic mirrors (DM2 and DM3) split the scattered light into three spectral domains. Bandpass filter 1 (BP1, 679DF6, Omega Optical) selects the 1055 cm^{-1} benzene ring Raman mode of 4-mercaptobenzoic acid (MBA; green detector). BP2 (713DF6, Omega Optical) selects a small spectral region without any Raman line for MBA (gray detector); this channel monitors the strength of the continuum background. A third channel has an OD 3.0 neutral density filter and monitors the Rayleigh scattering from the particles (red detector).

Photons detected by avalanche photodiodes (APDs, SPCM-AQR-14, PerkinElmer Optoelectronics) send TTL pulses to the counter timer card (PCI-6602, National Instruments) which records them with 12.5 ns time resolution, and stores them in the computer. Figure 1b shows the SERS spectrum of MBA attached to Ag nanoparticles overlaid with spectral ranges selected by filters for the three detectors. Figure 1c shows a typical intensity time trace with 10 ms time resolution showing individual Au nanoparticle scattering centers traversing the optical detection volume. The three channels shown correspond to the three detectors in Fig. 1a: green for the Raman line, black for the continuum background, and red for Rayleigh scattering. As can be seen, signal strength is often very strong, with thousands of photons detected per single burst. The three detectors and the associated timing electronics are used to record arrival times of scattered photons with 12.5 ns resolution, forming three photon streams, $I_{\mathrm{Rm}}(t)$, $I_{\mathrm{Ry}}(t)$, and $I_{\mathrm{Bkgd}}(t)$. These photon streams are analyzed by searching for photon bursts and calculating ratiometric observables, as well as performing auto- and cross-correlation analyses.

2.3 Ratiometric analysis of photon bursts

A burst of scattered photons from individual scattering clusters or particles is found using the algorithm described in Ref. [15], and provides start and end times t_{start} and t_{end}. The number of photons from each channel is integrated over this time to obtain a total number of photons per burst: $N_{\mathrm{Rm}} = \int_{t_{\mathrm{start}}}^{t_{\mathrm{end}}} I_{\mathrm{Rm}}(t)\,dt$, with similar definitions for N_{Ry} and N_{bkgd}. Two ratiometric variables quantify the relative intensities of the Rayleigh, Raman, and continuum background scattering. First,

$$r_1 = N_{\mathrm{Rm}} \Big/ \left(N_{\mathrm{Ry}} + N_{\mathrm{Rm}}\right) \qquad (1)$$

compares the number of photons detected that are from Raman scattering to those from Rayleigh scattering (note that the Rayleigh scattering APD had a neutral density filter with OD 3.6). Second,

$$r_2 = N_{\mathrm{Rm}} \big/ N_{\mathrm{bkgd}} + N_{\mathrm{Rm}} \qquad (2)$$

compares the number of photons that are from Raman scattering to those from . a small region of the continuum background (the "background" channel does not contain a Raman line for MBA),.

Both r_1 and r_2 are expected to increase upon functionalization of the nanoparticles with MBA or ABT due to the increasing contributions from Raman scattering. As can be seen from the time trace in Figure 1c, signals from all sources are of the same order of magnitude, with the Raman signature, when present, typically reflecting the strongest signal. Thus, $r_{\mathrm{Ry}}^{\mathrm{Rm}}$ and $r_{\mathrm{bkgd}}^{\mathrm{Rm}}$ are typically close to zero in the absence of a Raman signal, and otherwise reflect the strength of Rayleigh or continuum background signals relative to the Raman contribution. Pure Raman signals with no contributions from other signals will result in a ratio of 1, while increasing contributions will result in the ratio approaching zero. Note that the Raman channel can also contain a small contribution from continuum background scattering, because of its broad spectrum, so that this ratio is not 0 in the absence of a Raman-active molecules. Details of the behavior of these variables will be discussed below.

2.4 Correlation Spectroscopy

Correlation spectroscopy of individual photon bursts is performed as described in Ref. [15]. Correlation spectroscopy on SERS, background scattering, and Rayleigh scattering signals of nanoparticles provides rotational and translational diffusion parameters of particles. These can be interpreted in terms of the size of the scattering particles or clusters if the particles tend to from aggregates. As we will demonstrate, it will also allow us to distinguish between anisotropic scattering from particle-particle junctions and more isotropic scattering from individual nanoshells.

The following model was used to fit the individual correlations:

$$C(\tau) = c\left\{1 + \frac{1}{N\left(1+\tau/\tau_D\right)}\left[1 + \frac{A_P}{1-A_P}\exp\left(-\tau/\tau_P\right)\right]\right\} \qquad (3)$$

τ_D is the translational diffusion time, τ_P is the rotational diffusion time, and A_P is the relative amplitude of the rotational diffusion component. Rotational diffusion decays are in general multi-exponential. However, we assume a spherical particle, which leads to only two timescales, one of which dominates [16]. N is the number of particles in the detection volume, and c is a correction factor required to fit the correlations from individual particles [15].

A modification of the experimental setup in figure 1 is used to probe the origin of the two characteristic time scales found in correlations – one reflecting translational diffusion, the other one reflecting rotational diffusion. In this case, only two APDs are used, and a polarizing beam splitter cube is used rather than dichroic mirrors. The initial polarization of the laser beam is now carefully chosen to be linear. Polarization-FCS measures a polarization response and rotational diffusion times, both of which are indicative of nanoparticle clustering, because individual nanoparticles do typically exhibit rotational symmetry unless their shape is non-uniform (see discussion below).

3 Results and Discussion

3.1 Ratiometric Single Cluster Spectroscopy monitors homogeneity of SERS response

We first characterized the nanoparticle scattering properties using the ratios r_1 (comparing Raman and Rayleigh scattering) and r_2 (comparing Raman scatteringand continuum background). Both ratios expected to increase as the concentration of MBA is increased (Fig. 2a). The two-dimensional histograms in Figure 2 show the number of photon bursts as a function of r_1 and r_2 for the solid Ag, solid Au, and Au nanoshell samples. As can be seen from these histograms, Au nanoshell samples and Ag samples linked with ABT exhibit a significantly more homogeneous scattering response than the randomly aggregated solid Ag or Au samples.

The Ag nanoparticles used in this study are not of uniform size or shape, but they have been frequently used in studies showing very large Raman enhancements [1, 2, 17]. In the original unmodified samples, i.e. without addition of MBA, we observe a large number of scattering centers with significant Rayleigh scattering, and relatively little Raman scattering or continuum background scattering. This is shown by the large number of bursts with r_1 near 0 in Fig. 2b. Even so, as can be seen from this figure, there are quite a few scattering particles that show large signals (r_1>0) in the Raman and Continuum Background channels. This suggests that for a fraction of silver nanoparticles, no Raman-active molecules have to be attached to the nanoparticle surface to observe continuum background scattering; however, this does not exclude the possibility that Raman-active molecules can enhance the continuum background [17]. Figure 2e shows the distribution plot for particles that were incubated with 10 µM MBA, which leads to the emergence of a new subpopulation in the upper right-hand corner of the plot, with high r_1 and r_2 values. The scattering in this subpopulation is dominated by the SERS signal from MBA on the surface and shifts the distribution to higher values. Interestingly, the r_2 value also changes to higher values exhibiting a much narrower distribution than before. Clearly, a fraction of particles has

become SERS active, but it is also quite apparent that the large majority remains inactive despite the high MBA concentration added to the nanoparticle solution. As even more MBA is added (Fig. 2h), aggregation of the nanoparticles increases greatly (as will be further corroborated by their polarization response which will be addressed further below), and the SERS signal increases to the point, where now most of the particles have become SERS-active.

By linking this type of nanoparticle with a bifunctional linker ABT, we see that r_1 and r_2 are very close to 1, indicating consistent, strong Raman signals (ABT has a Raman mode similar to that of MBA at 1055 cm^{-1}). Although the shape and size of these nanoparticles are not uniform, a much more uniform response is obtained due to the controlled spacing provided by the linker.

Our Au nanoparticles are of much more uniform size and shape than Ag nanoparticles, as evidenced by transmission electron microscopy (data not shown). Surprisingly, however, in the case of Au nanoparticles, we observe a very different initial response from the bare particles (Figure 2c). Two subpopulations are clearly visible: one with very little Raman or Continuum Background scattering (low r_1), and one with significant Raman or CB (r_1 between 0.7 and 1.0). We find an overall weaker signal for the continuum background of Ag compared to Au. Particles incubated with MBA (Figures 2f and 2i) exhibit peak shifts for Raman and CB to higher r_2 values. This is because the Raman line from MBA now appears, and the intensity in the channel monitoring that line increases. Note, that the increase in r_2 is not as dramatic in this case as in the case of Ag. This is expected, since Ag in general provides larger SERS enhancements [18].

For the Au nanoshells (Figs. 2d, 2g, 2j), r_2 increases with MBA as with the solid Au nanoparticles. However, one significant difference is that there is only *one* subpopulation visible. The distribution in r_1 is relatively wide, but it does not split into two distinct subpopulations. This is likely due to the more homogeneous nature of the scattering nanoshells. Also, note that upon addition of MBA, the distribution of r_2 exhibits a rather subtle shift compared to both of the bulk nanoparticles.

In order to see a significant scattering signal from a nanoparticle, the electric field at the particle must be enhanced compared to the incident electric field both at the laser excitation frequency, g_0 (at ω_0), and at the Raman-shifted frequency, g (at $\omega_0 - \Delta$) [19]. We have recently shown, that surface-enhanced Raman scattering can be observed even from individual nanoshells [7], which is mostly due to their relatively wide surface plasmon resonance, which encompasses both the laser wavelength of 633 nm and the Raman shifted wavelength. The plasmon resonances of individual solid Ag and Au nanoparticles in contrast are not wide or strong enough. In order to obtain detectable signals in these cases, inter-particle junctions are necessary. Such plasmon resonances of inter-particle junctions caused by aggregation are very difficult to control, leading us to expect wider distributions in the ratios r_1 and r_2. We believe that the large population of solid nanoparticles with low r_1 (comparing Raman and Rayleigh scattering) are particle aggregates that show strong plasmon resonances at ω_0, but much weaker at $\omega_0 - \Delta$. The nanoshells, however, showed a more uniform response because of the better control over the plasmon resonance [8].

In Figure 3, we examine the widths of the distributions from Figure 2 more quantitatively, showing that the nanoshells produce narrower distributions in r_1 and r_2. In Figures 3a-c, one-dimensional histograms of r_2 are shown for all bursts with a large Raman component. Note that the widths of the histograms for nanoshells are narrower than the ones for solid particles - especially after adding MBA. r_2 is highest for Ag, consistent with the fact that it gives the largest SERS signals. Histograms for pure Ag particles are also most erratic, probably due to larger variations in shape. We attribute the fact that the histogram for Ag exhibits a wider distribution after the addition of high amounts of MBA (50 μM) to aggregation (sizing by rotational diffusion measurements below supports this claim).

In Figure 3d-e, we show the mean and standard deviation of the ratios r_1 and r_2 for all bursts, without selection of large Raman signals. Based on these plots it is obvious that the response of the nanoshells is typically more homogeneous exhibiting lower standard deviation in all cases. Even if we select only those bursts that show a large Raman signal (Figure 2f), the widths of the histograms for the nanoshells

are lower before and after the addition of MBA. Note that the narrowing of the distribution for Ag at high MBA concentrations is due simply to its high value of the ratio r_{bkgd} [11].

3.2 Heterogeneity monitored by sensitivity to laser polarization

The temporal response of SERS from individual nanoparticles may be analyzed using SERS correlation spectroscopy, similar to fluorescence correlation spectroscopy (FCS) [12]. Interestingly, the correlation response in SERS experiments on diffusing nanoparticles exhibits two characteristic time scales (Figure 4a-c). The longer time scale is indicative of translational diffusion of the nanoparticles through the confocal detection volume, and the shorter time scale is due to rotational diffusion of the nanoparticles. The rotational diffusion is only visible if the plasmon resonance of the nanoparticle is preferentially excited along a certain direction. Such a preferred direction may arise due to varying shapes of particles or by particle aggregation, e.g. dimer formation. For truly spherically symmetric particles, no sensitivity to polarization is expected.

When the laser excitation is polarized along the preferred dipole axis of a nanoparticle or nanoparticle cluster, a larger scattering signal is observed, whereas it is much weaker if the laser beam is polarized perpendicular to the particle dipole (Figure 4b). To identify the different diffusion time scales we split the emission into two channels with perpendicular polarization, and monitored the fluctuation time scales by performing auto- and cross-correlations between the two signals (Fig. 4c). For the shorter timescale, the autocorrelations of both polarizations had amplitudes larger than for the cross-correlations. This indicates a polarization-sensitive fluctuation from rotational diffusion of the nanoparticles. Similar identification of rotational diffusion was previously found with spherical Ag nanoparticles [12]. Having identified the translational and rotational diffusion components, we now analyze the heterogeneity of the sample on a particle-by-particle basis.

The nanoparticle samples we studied show distinct characteristics when monitored with correlation spectroscopy. By applying recently developed single-molecule FCS analysis methods [15] to SERS we can now determine the correlations from individual nanoparticles or nanoparticle clusters. In Figures 4b-d, we show examples of the autocorrelation function of the Rayleigh (red) and the Raman (black) channels as well as their cross-correlations (green and blue) for individual nanoparticles or nanoparticle clusters. In all cases, autocorrelations and cross-correlations of the Raman and Continuum Background channels overlap within expected error (data not shown). This agrees with previous observations that the continuum background and Raman signals appear to turn on and turn off together [17]. This method of particle scattering analysis is particularly powerful, because it enables us to simultaneously analyze the polarization response of Rayleigh and Raman signals from a single scattering center and determine if their behaviors are correlated or not. It further allows us to perform a statistical analysis of the results obtained from many individual scattering centers, rather than averaging the response of all particles into a single correlation plot.

Figure 4b shows typical results for particle assemblies of Ag nanoparticles. Both the Raman (black) and Rayleigh (red) channel autocorrelations show strong rotational diffusion contributions, and the cross-correlations show similar contributions, indicating that the Rayleigh and Raman dipoles are relatively well aligned with respect to each other. Results for the Ag nanoparticles linked with ABT are similar in appearance to those found using the randomly aggregated nanoparticles, except with longer timescales.

As shown in Figure 4c, Au nanoparticles exhibit a different behavior. First, the amplitudes of the rotational diffusion components are smaller than for the Ag nanoparticles in the autocorrelations. Second, the cross-correlations often have negative amplitudes, indicating that the strongest dipole directions for Rayleigh and Raman scattering may not overlap. These two facts indicate that there are multiple strong scattering interfaces in each nanoparticle assembly, with one stronger for the Rayleigh signal and another stronger in the Raman signal.

The Au nanoshells, however, exhibit yet another, very distinctive behavior (Figure 4d). Here, the rotational diffusion component of scattering is not detectable. This is indeed the expected behavior for a spherically symmetric scattering nanoparticle. A previous study claimed that the rotational

diffusion component could be seen with individual, spherically symmetric nanoparticles [12]. We were, however, not able to observe SERS scattering from solid nanoparticles without at least some degree of aggregration [8], which combined with the data shown here provides further strong evidence, that single particle SERS signals can only be obtained from special nano-engineered scattering structures, such as nanoshells. Solid particles require aggregation, i.e. at a minimum the formation of a particle dimer [4, 7].

3.3 Sizing nanoparticles using rotational diffusion time

By analyzing single burst correlations, such as the ones shown in Figure 4b-d, we can extract two size-related parameters from these correlations: the translational diffusion and rotational diffusion time scales. Figure 5 shows histograms of single burst parameters obtained from many particle burst correlations individually. Results for each type of particle are shown in columns: the results for the Ag nanoparticles are on the left, those for the Au nanoparticles are in the middle, and those for the Au nanoshells are shown on the right. For each nanoparticle or cluster, three parameters extracted from single burst analysis are shown: the translational diffusion time (top row, Figs. 5a-c), the rotational diffusion time (middle row, Figs. 5d-f), and the ratio of the rotational diffusion correlation amplitudes of the cross-correlations to that of the autocorrelation (bottom row, Figs. 5g-i). In each case, histograms are shown for increasing MBA concentration from black, to red, to green.

For the translational diffusion times, the Ag particles have the fastest diffusion (indicating smaller size), and the Au solid and shell particles have similar diffusion times. For the highest MBA concentration of 50 μM, there is wide distribution of translational diffusion times, indicating aggregation. The translational diffusion time depends on the diffusion constant according to,

$$\tau_D = \frac{\omega^2}{4D} = \frac{\omega^2 3\pi\eta}{4k_B T} l \qquad (4)$$

The particle is assumed to be spherical, so that the diffusion constant is $D = k_B T / 3\pi\eta l$. ω is the waist of the Gaussian confocal detection volume. η is the dynamic viscosity of water, and l is the diameter of the spherical particle. Hence the translational diffusion time can be used to size particles. However, the sizing depends on the size of the confocal detection volume which can vary due to alignment and must be carefully calibrated. More importantly, the diffusion time does not depend strongly on size, and, in the end, does not provide much information on the size.

For the rotational diffusion times, we again see that the Ag particles have the fastest diffusion (indicating smaller size). However, now we are not able to obtain reliable diffusion times for the NS sample, except in the case of the highest MBA concentration of 500 μM, where presumably some aggregation is occurring. The rotational diffusion times observed for the NS samples at lower concentrations varied over the whole range of possible values. As seen in Figs. 5g-I, clustering of the values was evident for Ag and Au solid particles, but the NS sample had lower values for A_P, indicating a weak rotational diffusion component. The exception is for 500 μM MBA, where some clustering of the values is evident. The dominant rotational diffusion time depends on the rotational diffusion constant Θ according to,

$$\tau_P = \frac{1}{6\Theta} = l^3 \frac{\pi\eta}{6k_B T} \qquad (5)$$

Again, the particle (or cluster) is assumed to be spherical, so that $\Theta = \frac{k_B T}{\pi\eta l^3}$. In general, rotational diffusion decays measured by correlation spectroscopy are multi-exponential [20]. Even for a sphere, there are two time scales [16]. However, in this case, one time scale dominates, and we use that here. In comparison to translational diffusion, the most important features are the much stronger dependence on size (cubic in diameter *l*, rather than linear), and the lack of dependence of confocal detection volume size.

We can use the rotational diffusion time to estimate the size of the particles. In Fig. 6a-b, we performed simulations of 50 and 100 nm particles diffusing in solution, and fit individual bursts using the same procedure we used in Fig. 5. Fitting the histograms to a lognormal distribution, we obtain estimates τ_P of 22 ± 2 μs for the 50 nm simulated particles and of 180 ± 10 μs for the 100 nm simulated particles. Using Eq. (5) above, we get sizes of 56 ± 5 nm and 110 ± 5 nm using rotational diffusion. The values may be biased upward due to the presence of the translational-diffusion induced fluctuations at similar timescales.

For translational diffusion, we obtain time scales of 6.4 ± 0.7 ms for the 50 nm simulated particles and 16 ± 3 ms for the 100 nm simulated particles. In our simulation, we used a non-Gaussian detection volume designed to approximate an actual detection volume [21]. Using Eq. (4) with ω = 500 nm, we get sizes of 45 ± 5 nm and 110 ± 20 nm. Even in this simple simulated sample, the variability found with the translational diffusion time is considerably more than with the rotational diffusion time (compare sensitivity of both methods in Fig. 6c). In addition, there is the added complication of calibration of detection volume size with translational diffusion measurements.

In Fig. 6d, we show the dependence of rotational diffusion time on effective particle diameter, and plot the fitted values for the data from Fig. 5. The mean size of each sample is determined. These sizes match well the sizes for these systems mentioned in Materials and Methods. The increase in size and variability is particularly evident in the Ag nanoparticle sample (not shown since it fitted size was 220 nm), due to aggregation upon addition of 50 μM MBA. The average size of Ag nanoparticles linked with ABT was measured to be above 100 nm.

4 Conclusion

We have demonstrated the utility of solution-based single-particle techniques for characterization of the heterogeneity of SERS-active substrates. The engineered nanostructures have been shown to produce more consistent response that random aggregation, validating these approaches for improving SERS response of nanoparticle systems. We believe these techniques will prove useful for more rapidly improving these characteristics in future work.

ACKNOWLEDGMENTS

This work performed under the auspices of the U.S. Department of Energy by Lawrence Livermore National Laboratory under Contract DE-AC52-07NA27344. Funding from the Institute for Collaborative Biotechnologies (ICB) through Grant DAAD19-03-D-0004 from U.S. Army Research Office to N Reich.

REFERENCES

1. Kneipp, K.; Yang, W.; Kneipp, H.; Perelman, L. T.; Itzkan, I.; Dasari, R. R.; Feld, M. S. *Physical Review Letters* **1997,** 78, (9), 1667-70.
2. Nie, S.; Emory, S. R. *Science* **1997,** 275, (5303), 1102-6.
3. Aravind, P. K.; Nitzan, A.; Metiu, H. *Surface Science* **1981,** 110, (1), 189.
4. Hongxing Xu, M. K. *ChemPhysChem* **2003,** 4, (9), 1001-1005.
5. Xu, H.; Aizpurua, J.; Kall, M.; Apell, P. *Phys Rev E Stat Phys Plasmas Fluids Relat Interdiscip Topics* **2000,** 62, (3 Pt B), 4318-24.

6. Michaels, A. M.; Nirmal, M.; Brus, L. E. *Journal of the American Chemical Society* **1999,** 121, (43), 9932-9939.
7. Talley, C. E.; Jackson, J. B.; Oubre, C.; Grady, N. K.; Hollars, C. W.; Lane, S. M.; Huser, T. R.; Nordlander, P.; Halas, N. J. *Nano Lett* **2005,** 5, (8), 1569-74.
8. Schwartzberg, A. M.; Oshiro, T. Y.; Zhang, J. Z.; Huser, T.; Talley, C. E. *Anal Chem* **2006,** 78, (13), 4732-6.
9. Bishnoi, S. W.; Rozell, C. J.; Levin, C. S.; Gheith, M. K.; Johnson, B. R.; Johnson, D. H.; Halas, N. J. *Nano Lett* **2006,** 6, (8), 1687-92.
10. Weiss, S. *Science* **1999,** 283, (5408), 1676-83.
11. Dahan, M.; Deniz, A. A.; Ha, T.; Chemla, D. S.; Schultz, P. G.; Weiss, S. *Chemical Physics* **1999,** 247, (1), 85-106.
12. Eggeling, C.; Schaffer, J.; Seidel, C. A. M.; Korte, J.; Brehm, G.; Schneider, S.; Schrof, W. *J. Phys. Chem. A* **2001,** 105, (15), 3673-3679.
13. Lee, P. C.; Meisel, D. *Journal of Physical Chemistry* **1982,** 86, (17), 3391-3395.
14. Jana, N. R.; Gearheart, L.; Murphy, C. J. *Chem. Mater.* **2001,** 13, (7), 2313-2322.
15. Laurence, T. A.; Kwon, Y.; Yin, E.; Hollars, C. W.; Camarero, J. A.; Barsky, D. *Biophys. J.* **2007,** 92, (6), 2184-2198.
16. Aragón, S. R.; Pecora, R. *Biopolymers* **1975,** 14, (1), 119-137.
17. Jiang, J.; Bosnick, K.; Maillard, M.; Brus, L. *J. Phys. Chem. B* **2003,** 107, (37), 9964-9972.
18. Moskovits, M. *Reviews of Modern Physics* **1985,** 57, (3), 783-826.
19. Kerker, M.; Wang, D. S.; Chew, H. *Applied Optics* **1980,** 19, (24), 4159-4174.
20. Aragon, S. R.; Pecora, R. *Journal of Chemical Physics* **1976,** 64, (4), 1791-803.
21. Laurence, T. A.; Kapanidis, A. N.; Kong, X. X.; Chemla, D. S.; Weiss, S. *Journal of Physical Chemistry B* **2004,** 108, (9), 3051-3067.

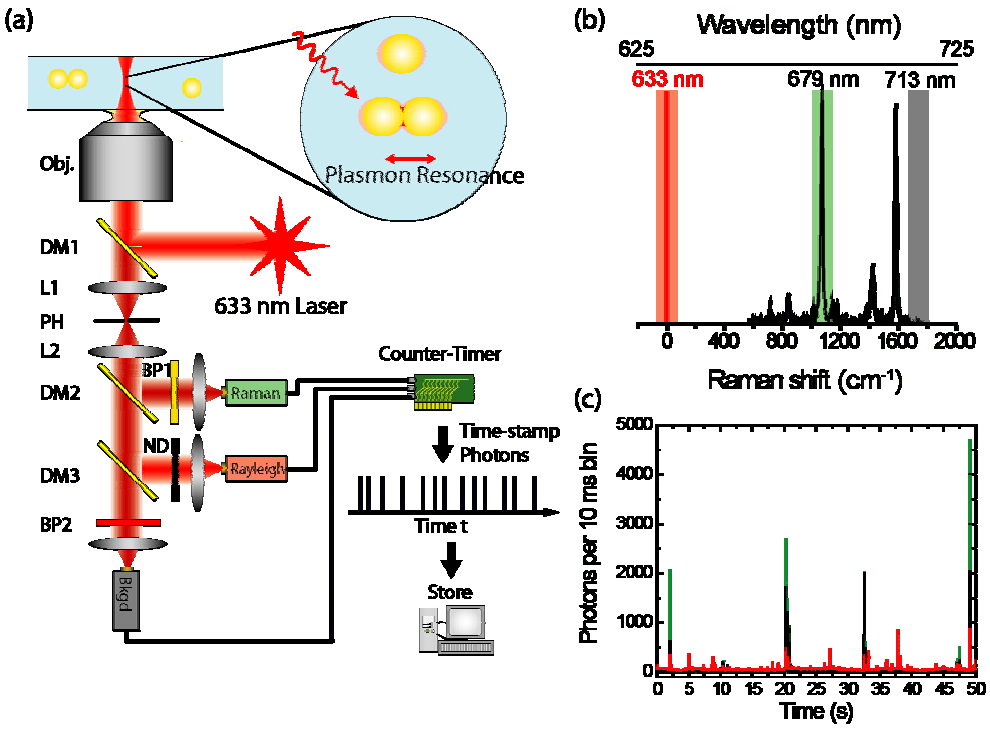

Figure 1: Homogeneity of size and optical response of metal nanoparticles is probed using solution-based ratiometric single particle and cluster spectroscopy. (a) Experimental setup. Individual metallic nanoparticles and clusters of nanoparticles are allowed to freely diffuse in solution. Bursts of photons scattered by nanoparticle clusters diffusing through the laser spot are collected and split into three spectral domains isolating the 1055 cm^{-1} benzene ring breathing Raman line of 4-mercaptobenzoic acid (MBA; green detector), the continuum background (gray detector), and Rayleigh scattered light from the particles (red detector). A counter timer card records photon events from each detector with 12.5 ns time resolution. (b) SERS spectrum of MBA on Ag nanoparticles overlaid with spectral ranges selected by filters for the three detectors. (c) Time trace with 10 ms time resolution showing individual Au nanoparticle scattering centers traversing the optical detection volume. The three channels shown correspond to the three detectors in part (a): green for the Raman line, black for the continuum background, and red for Rayleigh scattering.

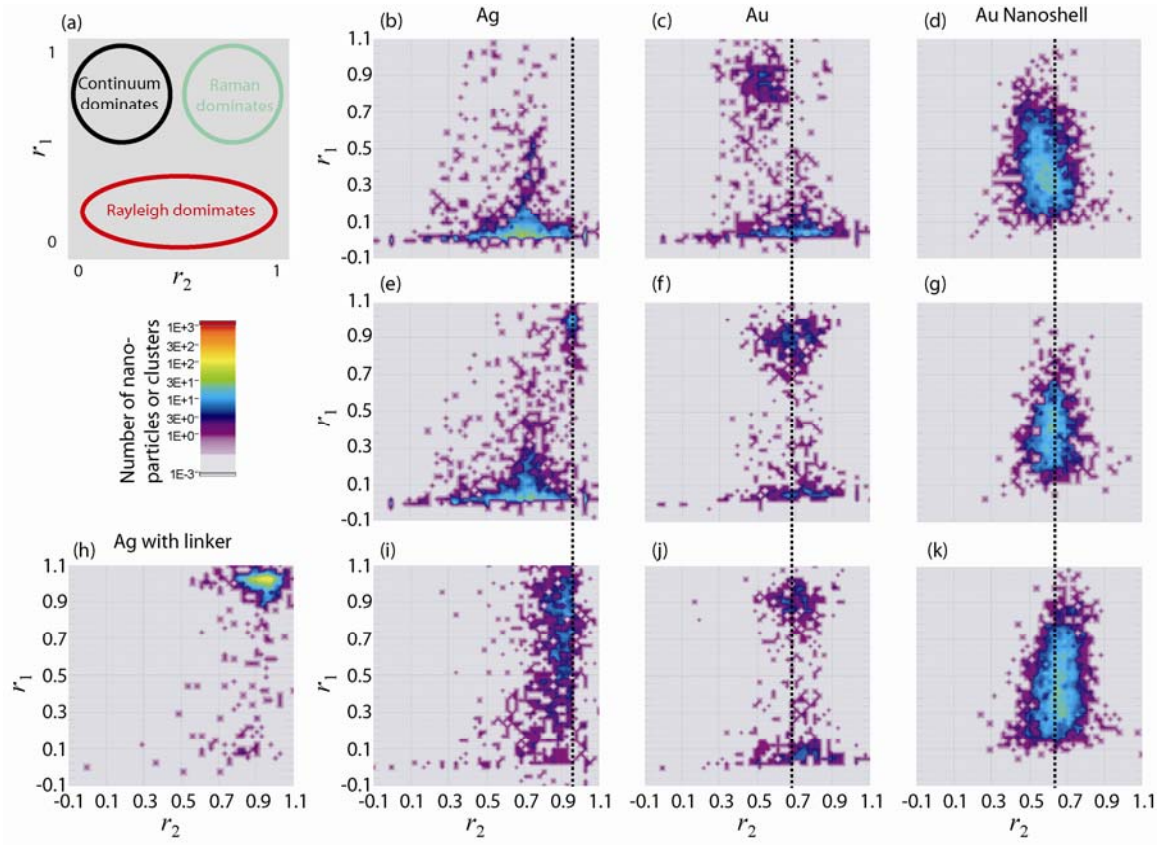

Figure 2: Two-dimensional histograms of single nanoparticles or clusters compare strengths of Raman scattering, Rayleigh scattering, and the continuum background signal. Ratiometric variables r_1 and r_2 calculated for single diffusing clusters or particles are used to monitor the effects of functionalizing the nanoparticles with 4-mercaptobenzoic acid (MBA). (a) The ratio r_1 compares the strength of the Raman scattering to the Rayleigh scattering (Rayleigh scattering is attenuated by a neutral density filter). For r_1 near 0, Rayleigh scattering dominates, whereas, for r_1 near 1, Raman scattering dominates the signal. The ratio r_2 compares the strength of the Raman scattering to the continuum background in a similar manner. Histograms for Ag nanoparticles with 0, 10, and 50 μM MBA are shown in (b), (e), and (i), respectively. Histograms for Au nanoparticles with 0, 10, and 50 μM MBA are shown in (c), (f), and (j), respectively. Histograms for Au nanoshells (size, synthesis) with 0, 50, and 500 μM MBA are shown in (d), (g), and (k), respectively. The histogram for Ag nanoparticles linked with ABT, and polymer coated is shown in (h). The dotted lines indicate the position in r_2 of the Raman active subpopulation at the intermediate MBA concentration for each substrate. The position of Raman active subpopulation shifts to the right as MBA is added. Inducing aggregation by adding NaCl does causes a smaller shift in the opposite direction (data not shown).

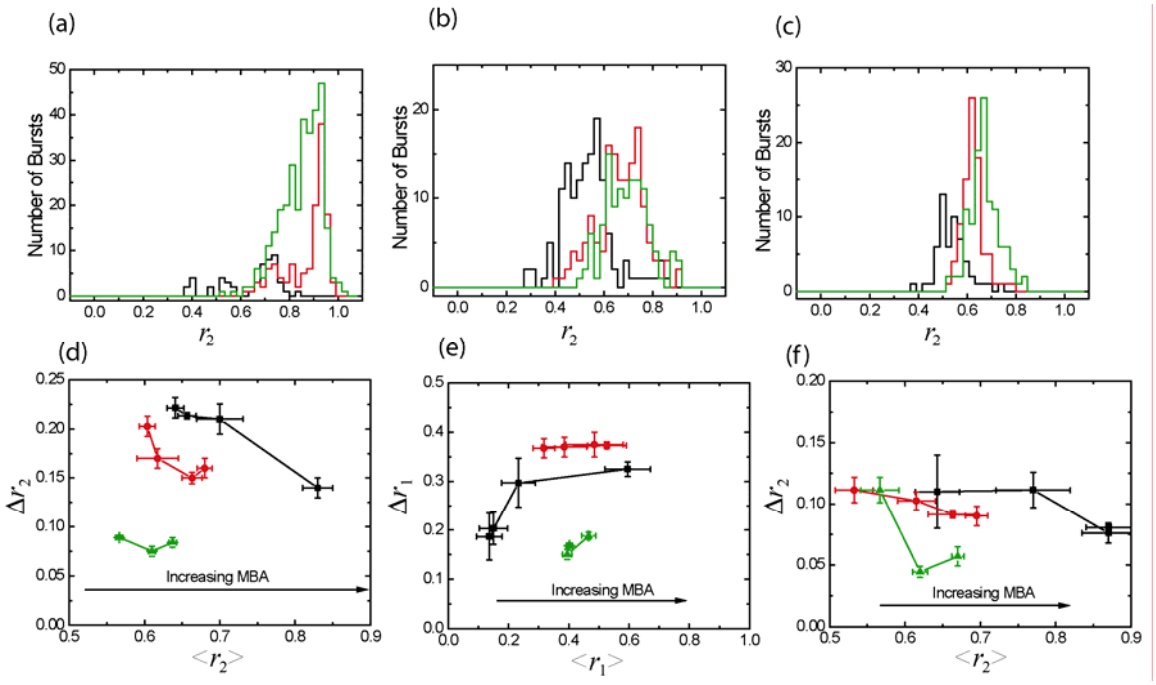

Figure 3: Histograms of ratiometric variables r_2 (comparing Raman to continuum background) calculated for single diffusing nanoparticle clusters with bright Raman signal (>15 kHz) selected from histograms in figure 2. (a) Histograms for Ag nanoparticles at 0 (black), 10 (red), and 50 μM MBA (green). (b) Histograms for Au nanoparticles at 0 (black), 10 (red), and 50 μM MBA (green). (c) Histograms for Au nanoshells at 0 (black), 50 (red), and 500 μM MBA (green). (d) Fitted peak position and width for histograms of r_2 from figure 2. For Ag nanoparticles (black), MBA concentrations from left to right are 0, 1, 10, and 50 μM. For Au nanoparticles (red), MBA concentrations from left to right are 0, 1, 10, and 50 μM. For Au nanoshells (green), MBA concentrations from left to right are 0, 50, and 500 μM. (e) Fitted peak position and width for histograms of r_1 (comparing Raman to Rayleigh scattering) from figure 2, similar to (d). (f) Fitted peak position and width for histograms of r_2 from bright Raman signals of parts (a), (b) and (c).

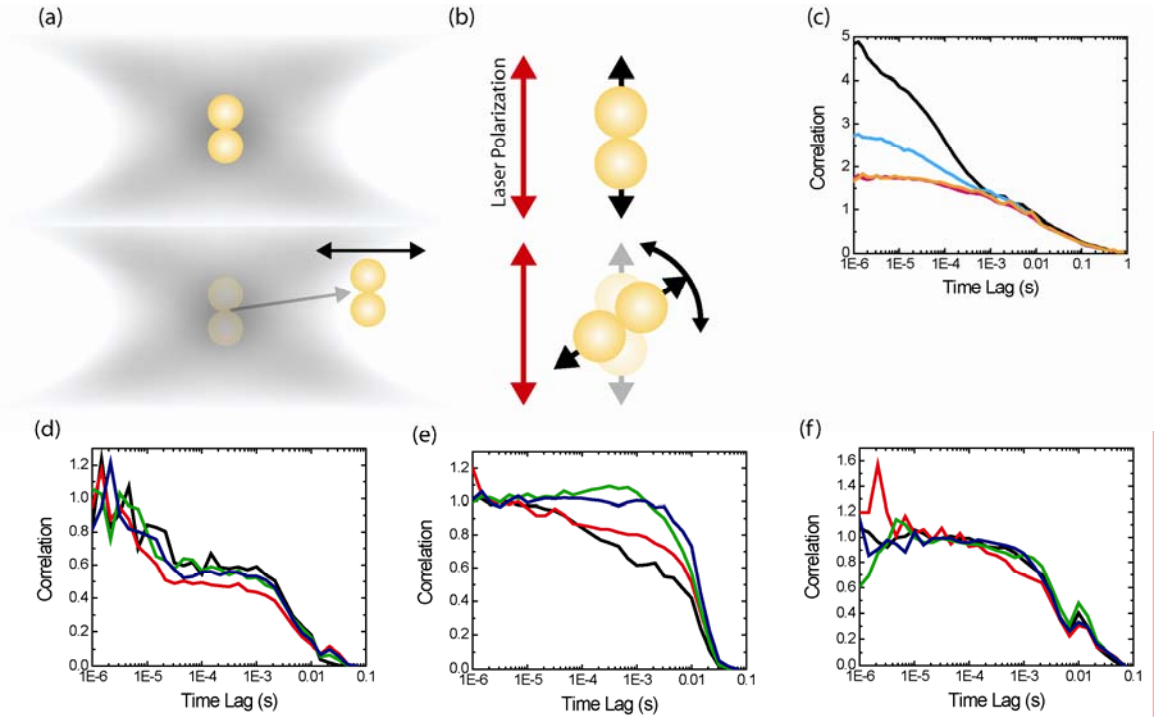

Figure 4: Translational diffusion and rotational diffusion both affect correlation spectroscopy signals. (a) Translational diffusion of nanoparticles into and out of the confocal detection volume produces intensity fluctuations. (b) Rotational diffusion of polarization-sensitive nanoparticle clusters produces intensity fluctuations. The time scale of fluctuations induced by translational diffusion depends on size of confocal detection volume, but the time scale for rotational diffusion does not. (c) These two time scales are evident in correlations from nanoparticles diffusing in solution, and are identified using polarization sensitive detection. Scattering signals from nanoparticles are monitored using two channels, one with polarization parallel to the excitation, and one perpendicular to the excitation. Autocorrelations of the parallel (black) and perpendicular (cyan) channels are shown, as well as cross-correlations of the two channels (orange and magenta). The longer timescale reflects translational diffusion and does not depend on polarization. The shorter timescale is due to rotational diffusion. The ability to detect rotational diffusion depends on the anisotropic polarization dependence of plasmon excitations due to clustering of nanoparticles. For nanoshells, the rotational diffusion fluctuations are absent due to their isotropic surface plasmon response. Using the information that the second correlation timescale is due to rotational diffusion, we can study the relative orientation of Raman-active and Rayleigh-active dipoles in samples. Representative correlations from *single bursts* are shown after expanding the correlation region. (b) Correlations for a single Raman active Ag scattering center. Autocorrelation of Raman signal (black), autocorrelation of Rayleigh signal (red), and the two cross-correlations of the Raman signal with the Rayleigh signal (green and blue) are shown. (c) Correlations for single Raman active Au scattering center. (d) Correlations for single Au nanoshell.

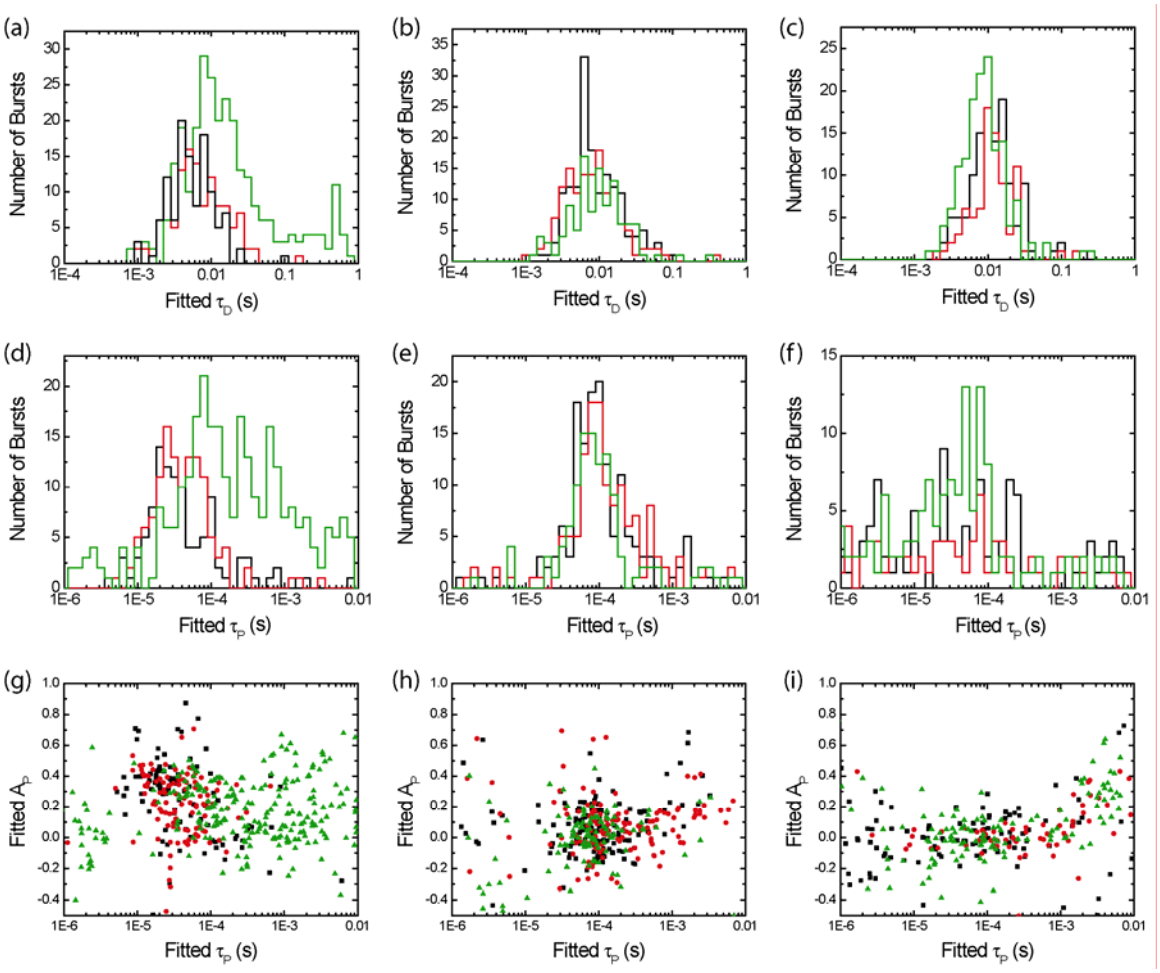

Figure 5: For each scattering center, a two component correlation spectroscopy model is fitted to the correlations from an individual burst of photons. It is a global fit of all four correlations shown in figure 4. The results are formed into histograms shown here, and the populations are fitted. (a) Histograms of fitted translational diffusion time τ_D for Ag nanoparticles with 0 (black), 10 (red), and 50 μM MBA (green). (b) Same as (a), but for Au nanoparticles. (c) Same as (a), but for Au nanoshells with 0 (black), 50 (red), and 500 μM MBA (green). (d-f) Same as (a-c), but now for histograms of fitted rotational diffusion time τ_P. (g-i) Scatter plots of the relative amplitude A_P of the polarization-related fluctuations for the cross-correlations versus the fitted rotational diffusion time τ_P. Samples and colors are same as in (a-c). If A_P is larger than 0, then there was a significant component of the polarization-related fluctuation found. If A_P is less than 0, that component was negative, indicating that the Raman-active and Rayleigh-active dipoles are not aligned, or are nearly perpendicular.

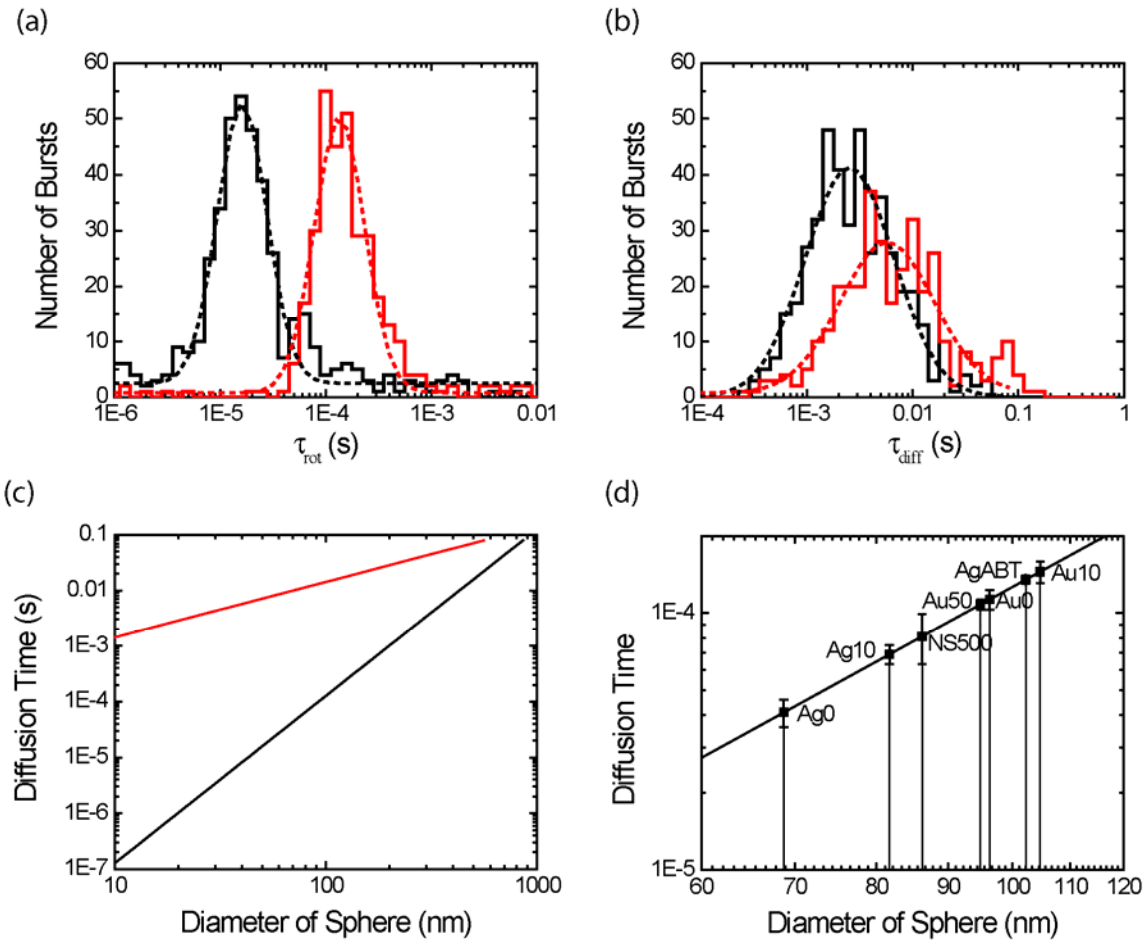

Figure 6: The rotational diffusion time constant can be used for sizing of metallic nanoparticles. (a) Fitted rotational diffusion times for *simulated* single particle scattering centers analogous to Figure 5. Each scattering center is assumed to be spherical, and to scatter only along one polarization axis. Black: 50 nm particles: red: 100 nm particles. Dotted lines: fits to lognormal model. Fitted widths were 0.54 ± 0.02 in natural logarithmic units. (b) The fitted translational diffusion timescales for same simulations; these are less sensitive to size of nanoparticles. Also, fitted widths are wider: 0.99 ± 0.06 in natural logarithmic units. (c) The sensitivity of rotational diffusion timescales to nanoparticle size (black line) is greater than the sensitivity of translational diffusion (red line). The translational diffusion timescale also depends on the size of the confocal detection volume. (d) The average sizes of the samples used in Fig. 5 are determined using their rotational diffusion time scales. Each experiment is labeled by the sample (Ag, Au, and NS, for Ag nanoparticles, Au nanoparticles, and Au nanoshells, respectively), and by MBA concentration in μM; Ag nanoparticles with ABT linker are denoted AgABT. The Ag nanoparticles with 50 μM MBA (size fitted was centered at 220 nm).